A&A 590, A129 (2016)
DOI: 10.1051/0004-6361/201628314

Astronomy & Astrophysics

Are long gamma-ray bursts biased tracers of star formation? Clues from the host galaxies of the *Swift*/BAT6 complete sample of bright LGRBs

II. Star formation rates and metallicities at $z < 1$[⋆,⋆⋆]

J. Japelj[1,2], S. D. Vergani[3,4,5], R. Salvaterra[6], P. D'Avanzo[4], F. Mannucci[7], A. Fernandez-Soto[8,9], S. Boissier[10], L. K. Hunt[7], H. Atek[11,12], L. Rodríguez-Muñoz[13,14], M. Scodeggio[6], S. Cristiani[1], E. Le Floc'h[15], H. Flores[3], J. Gallego[13], G. Ghirlanda[4], A. Gomboc[16,2], F. Hammer[3], D. A. Perley[17], A. Pescalli[4], P. Petitjean[5], M. Puech[3], M. Rafelski[18], and G. Tagliaferri[4]

[1] INAF–Osservatorio Astronomico di Trieste, via G. B. Tiepolo 11, 34131 Trieste, Italy
e-mail: japelj@oats.inaf.it
[2] Faculty of Mathematics and Physics, University of Ljubljana, Jadranska ulica 19, 1000 Ljubljana, Slovenia
[3] GEPI–Observatoire de Paris Meudon. 5 place Jules Jannsen, 92195 Meudon, France
[4] INAF–Osservatorio Astronomico di Brera, via E. Bianchi 46, 23807 Merate, Italy
[5] Institut d'Astrophysique de Paris, Université Paris 6-CNRS, UMR7095, 98bis boulevard Arago, 75014 Paris, France
[6] INAF–IASF Milano, via E. Bassini 15, 20133 Milano, Italy
[7] INAF–Osservatorio Astrofisico di Arcetri, Largo E. Fermi 5, 50125 Firenze, Italy
[8] Instituto de Física de Cantabria (CSIC-UC), 39005 Santander, Spain
[9] Unidad Asociada Observatori Astronómic (IFCA – Universitat de Valéncia), Valencia, Spain
[10] Aix Marseille Université, CNRS, LAM (Laboratoire d'Astrophysique de Marseille) UMR 7326, 13388 Marseille, France
[11] Laboratoire d'Astrophysique, École Polytechnique Fédérale de Lausanne, Observatoire de Sauverny, 1290 Versoix, Switzerland
[12] Department of Astronomy, Yale University, 260 Whitney Avenue, New Haven, CT 06511, USA
[13] Departamento de Astrofísica y Ciencias de la Atmósfera, Universidad Complutense de Madrid, 28040 Madrid, Spain
[14] Dipartimento di Fisica e Astronomia "G. Galilei", Università di Padova, Vicolo dell'Osservatorio 3, 35122 Padova, Italy
[15] Laboratoire AIM, IRFU/Service d'Astrophysique – CEA/DSM – CNRS – Université Paris Diderot, Bât. 709, CEA-Saclay, 91191 Gif-sur-Yvette Cedex, France
[16] Faculty of Sciences, University of Nova Gorica, Vipavska cesta 11c, 5270 Ajdovščina, Slovenia
[17] Dark Cosmology Centre, Niels Bohr Institute, University of Copenhagen, Juliane Maries Vej 30, 2100 Copenhagen, Denmark
[18] NASA Postdoctoral Program Fellow, Goddard Space Flight Center, Greenbelt, MD 20771, USA

Received 15 February 2016 / Accepted 4 April 2016

ABSTRACT

Aims. Long gamma-ray bursts (LGRBs) are associated with the deaths of massive stars and might therefore be a potentially powerful tool for tracing cosmic star formation. However, especially at low redshifts ($z < 1.5$) LGRBs seem to prefer particular types of environment. Our aim is to study the host galaxies of a complete sample of bright LGRBs to investigate the effect of the environment on GRB formation.

Methods. We studied host galaxy spectra of the *Swift*/BAT6 complete sample of 14 $z < 1$ bright LGRBs. We used the detected nebular emission lines to measure the dust extinction, star formation rate (SFR), and nebular metallicity (Z) of the hosts and supplemented the data set with previously measured stellar masses $M_\star$. The distributions of the obtained properties and their interrelations (e.g. mass-metallicity and SFR-$M_\star$ relations) are compared to samples of field star-forming galaxies.

Results. We find that LGRB hosts at $z < 1$ have on average lower SFRs than if they were direct star formation tracers. By directly comparing metallicity distributions of LGRB hosts and star-forming galaxies, we find a good match between the two populations up to $12 + \log\left(\frac{\mathrm{O}}{\mathrm{H}}\right) \sim 8.4$–$8.5$, after which the paucity of metal-rich LGRB hosts becomes apparent. The LGRB host galaxies of our complete sample are consistent with the mass-metallicity relation at similar mean redshift and stellar masses. The cutoff against high metallicities (and high masses) can explain the low SFR values of LGRB hosts. We find a hint of an increased incidence of starburst galaxies in the *Swift*/BAT6 $z < 1$ sample with respect to that of a field star-forming population. Given that the SFRs are low on average, the latter is ascribed to low stellar masses. Nevertheless, the limits on the completeness and metallicity availability of current surveys, coupled with the limited number of LGRB host galaxies, prevents us from investigating more quantitatively whether the starburst incidence is such as expected after taking into account the high-metallicity aversion of LGRB host galaxies.

Key words. gamma-ray burst: general – galaxies: star formation

⋆ Based on observations at ESO, Program IDs: 077.D-0425, 177.A-0591, 080.D-0526, 081.A-0856, 082.D-0276, 083.D-0069, 084.A-0303, 084.A-0260, 086.A-0644, 086.B-0954, 089.A-0868, 090.A-0760, 095.D-0560.
⋆⋆ The reduced spectra are available in the ESO archive as Phase 3 data products and in the GTC archive.

1. Introduction

Ever since long[1] gamma-ray bursts (LGRBs) were first linked to the explosions of very massive stars (Hjorth et al. 2003; Hjorth & Bloom 2012), they have been considered as promising tracers of star formation in galaxies to very high redshifts (e.g. Kistler et al. 2008; Robertson & Ellis 2012; Perley et al. 2016a; Greiner et al. 2015). LGRB host galaxies can be used as a complementary means to standard surveys of star-forming galaxies in order to understand galaxy properties and their evolution throughout cosmic history (e.g. Shapley 2011; Carilli & Walter 2013). Studying LGRB hosts presents important observational advantages over studying luminosity-selected galaxies. GRBs select galaxies independently of their brightness and thus avoid limitations (e.g. magnitude-limited samples, dust extinction, redshift incompleteness) that usually accompany galaxy surveys. In particular, GRBs can pinpoint the faintest galaxies up to high redshifts ($z > 6$; Tanvir et al. 2012; Basa et al. 2012; Salvaterra et al. 2013), a population that might be a fundamental contributor to the re-ionization (Salvaterra et al. 2011) but remains mainly elusive to conventional photometric and spectroscopic surveys.

To understand whether LGRB hosts can be used as a representative population of star-forming galaxies, we need to understand the link between the LGRB phenomena and star formation processes, in the following referred to as GRB (production) efficiency. Of particular interest is the behaviour of GRB efficiency with respect to the properties of GRB host environment, such as stellar mass ($M_\star$), star formation rate (SFR), and metallicity. Studies in the past have reached contradictory conclusions regarding the LGRB efficiency, largely because of the heterogeneous nature of investigated samples (e.g. Le Floc'h et al. 2003, 2006; Fruchter et al. 2006; Savaglio et al. 2009; Levesque et al. 2010a; Svensson et al. 2010; Mannucci et al. 2011; Graham & Fruchter 2013; Perley et al. 2013; Hunt et al. 2014). However, the large number of LGRBs detected by the *Swift* satellite (Gehrels et al. 2004) accumulated in the past ten years and carefully chosen selection criteria have recently resulted in several unbiased LGRB samples, highly complete in redshift: the GROND (Greiner et al. 2011), BAT6 (Salvaterra et al. 2012), TOUGH (Hjorth et al. 2012), and SHOALS (Perley et al. 2016a) samples. With the help of these samples a more complete picture of the population of LGRB hosts is being revealed.

At high redshifts very few galaxies are used in analyses, which is presumably the reason why the conclusions drawn from different unbiased samples still differ: while some studies (Greiner et al. 2015; Perley et al. 2016b) claimed that LGRB hosts can be direct tracers of star formation at about $z > 3$, others find the hosts to be of low luminosity with a metallicity-dependent efficiency (Schulze et al. 2015).

The picture is gradually becoming clearer at low redshifts ($z < 1.5$). Several studies have investigated the metallicity of hosts and its effect on GRB efficiency, especially since theoretical models for single LGRB progenitor stars have predicted a low metallicity threshold above which LGRBs could not occur (Yoon et al. 2006; Woosley & Heger 2006). The recent evidence, either direct (Krühler et al. 2015) or indirect (Vergani et al. 2015; Perley et al. 2016b; Schulze et al. 2015), from complete samples suggests that at low redshifts the LGRBs are indeed produced preferentially in low-metallicity environments. The metallicity threshold inferred from the data is $12 + \log\left(\frac{\mathrm{O}}{\mathrm{H}}\right) \sim 8.3$–$8.6$, confirming the findings of some of the previous studies focused on incomplete samples (Modjaz et al. 2008; Levesque et al. 2010a; Graham & Fruchter 2013). LGRB hosts at $z < 1$ are also found to be fainter and of lower stellar mass than a field star-forming galaxy population (see also Vergani et al. 2015; Perley et al. 2013, 2016b). Because the stellar mass and metallicity of star-forming galaxies are correlated (stellar mass-metallicity relation, Tremonti et al. 2004), the low-metallicity preference could provide the explanation for the differences in observed stellar masses between populations. Furthermore, SFR and stellar mass of star-forming galaxies are correlated (e.g. Brinchmann et al. 2004), therefore metallicity has also been suggested as a possible explanation for the observed preference towards low SFRs in the LGRB host population (Boissier et al. 2013; Krühler et al. 2015; but see Michałowski et al. 2012). However, metallicity may not be the only factor affecting the LGRB production efficiency (e.g. Kelly et al. 2014; Perley et al. 2015). Even though a number of studies have addressed this issue, no self-consistent study has been performed simultaneously on stellar masses, SFRs and metallicities of a complete sample of LGRBs hosts. This is the goal of our study of the *Swift*/BAT6 complete sample of bright LGRBs.

Recently, Vergani et al. (2015) presented a study on the photometry and stellar masses of the $z < 1$ LGRB host galaxies of the *Swift*/BAT6 complete sample of bright LGRBs. The *Swift*/BAT6 sample (Salvaterra et al. 2012) is selected according to favourable observing conditions (Jakobsson et al. 2006) to avoid a biased selection. To ensure a significant redshift completeness – the sample is 97% complete in redshift – LGRBs are furthermore selected by their brightness in gamma-rays (*Swift*/BAT peak flux $P \geq 2.6$ ph s^{-1} cm^{-2}). The selection requirements do not depend on the brightness of optical afterglows, ensuring that the sample contains the entire LGRB population, including dark LGRBs (Melandri et al. 2012). Vergani et al. (2015) found that $z < 1$ LGRBs preferentially select faint, low-mass star-forming galaxies and are not unbiased tracers of star formation at $z < 1$. To better understand the interdependency of key properties of galaxies hosting LGRBs, here we expand the work of Vergani et al. (2015) by studying the emission line spectra of the hosts in the complete sample. Using the emission line fluxes, we measure the star formation rates and metallicities of the BAT6 sample hosts (Sect. 3). We compare the distributions of $M_\star$, SFR, and metallicity and their interrelations (i.e. *SFR*-$M_\star$, mass-metallicity *MZ* relation) to those derived from other samples of star-forming galaxies. Particularly, we focus our analysis on the completeness of the different comparison samples and the effect of different sample selection criteria on the final results (Sect. 5).

All errors are reported at 1σ confidence unless stated otherwise. We use a standard cosmology (Planck Collaboration XVI 2014): $\Omega_\mathrm{m} = 0.315$, $\Omega_\Lambda = 0.685$, and $H_0 = 67.3$ km s^{-1} Mpc^{-1}. All quantities are computed with respect to the Chabrier initial mass function (Chabrier 2003).

2. Sample and data reduction

Our sample is the same as presented in Vergani et al. (2015) and is composed of 14 $z < 1$ LGRBs of the *Swift*/BAT6 sample (Salvaterra et al. 2012). Because it is difficult to maintain a high level of GRB host data completeness at high redshifts

[1] GRBs are traditionally classified as long and short according to their observed duration (i.e. longer or shorter than ~2 s). In contrast to long GRBs, short GRBs are believed to arise from a merger of a compact object binary system and are found to have older progenitors (e.g. Fong & Berger 2013).

Table 1. Details of the observations of GRB hosts in the sample.

GRB host	E^G_{B-V} (mag)	Date	Instrument	Exp. time (s)	Slit width* (″)	Dispersion (Å/pixel)	Wavelength range (Å)	Seeing (″)	Airmass	Reference
050416A	0.026	2011-01-19	VLT/X-Shooter	4 × 900/4 × 900/12 × 300	1.0/0.9/0.9	0.4/0.4/1.0	3000–25 000	0.7	1.5	(1)
050525A	0.083	2012-09-18	VLT/X-Shooter	4 × 630/4 × 664/4 × 695	1.0/0.9/0.9JH	0.4/0.4/1.0	3000–20000	1.5	1.6	(1)
060614	0.019	2006-07-23	VLT/FORS2	1 × 1500	1.0	3.3	3000–9600	1.2	1.2	(2)
		2007-04-26	VLT/FORS1	2 × 1200	1.3	1.5	3600–6000	0.8	1.5	(3)
060912A	0.046	2012-09-21	VLT/X-Shooter	2 × 900/2 × 934/2 × 965	1.3/1.2/1.2	0.4/0.4/1.0	3000–25 000	0.7	1.5	(1)
061021	0.051	2013-03-21	VLT/X-Shooter	12 × 940/12 × 900/36 × 320	1.0/0.9/0.9JH	0.4/0.4/1.0	3000–20000	0.9	1.1	(1)
071112C†	0.105	2007-11-13	VLT/FORS2	2 × 1800	1.0	3.3	3000–9500	1.0	1.7	(4)
080319B	0.010	2014-02-26	GTC/OSIRIS	4 × 825	1.23	2.6	5100–10 000	0.8	1.1	(3)
		2014-02-28	GTC/OSIRIS	4 × 825	1.23	2.6	5100–10 000	1.2	1.1	(3)
080430	0.011	2014-01-07	GTC/OSIRIS	8 × 825	1.23	2.6	5100–10 000	1.1	1.1	(3)
080916A	0.017	2008-09-17	VLT/FORS1	6 × 600	1.0	3.3	3000–9500	0.8	1.2	(4)
081007	0.014	2015-05-16	VLT/X-Shooter	4 × 700/4 × 700/12 × 250	1.3/1.2/1.2	0.4/0.4/1.0	3000–25000	1.0-2.1	1.2	(3)
		2015-06-20	VLT/X-Shooter	8 × 700/8 × 700/24 × 250	1.3/1.2/1.2	0.4/0.4/1.0	3000–25000	0.8-1.0	1.1	(3)
		2008-11-03	VLT/FORS2	3 × 2700	1.0	3.2	5700–10 000	0.5	1.1	(5)
090424	0.022	2009-05-22	VLT/FORS2	3 × 3600	1.0	3.2	6000–10 200	0.7	1.4	(5)
		2013-04-08	GTC/OSIRIS	3 × 800	1.23	2.1	3630–7500	0.9	1.1	(5)
091018†	0.026	2009-10-18	VLT/X-Shooter	4 × 600/4 × 600/4 × 600	1.0/0.9/0.9	0.4/0.4/1.0	3000–25 000	0.9	2.0	(6)
091127†	0.035	2010-02-12	VLT/X-Shooter	4 × 1500/4 × 1500/4 × 750	1.0/0.9/0.9	0.4/0.4/1.0	3000–25 000	1.0	1.1	(7)
100621A	0.027	2012-10-16	VLT/X-Shooter	2 × 1200/2 × 1200/8 × 300	1.0/0.9/0.9JH	0.4/0.4/1.0	3000–20000	0.9	1.3	(1)

Notes. For each GRB we report Galactic reddening in its line of sight and the information regarding the spectroscopic observation of its host galaxy: date of observation, telescope and instrument, instrumental setup (exposure time, slit widths, dispersion, wavelength range of the obtained spectrum), observing conditions (seeing and airmass), and the reference of the first published work presenting the spectrum. (*) 0.9JH stands for the X-Shooter near-infrared slits with a special K-blocking filter (Vernet et al. 2011). (†) Spectra are dominated by afterglow emission.

References. (1) Krühler et al. (2015); (2) Della Valle et al. (2006); (3) This study; (4) Fynbo et al. (2009); (5) Jin et al. (2013); (6) Wiersema et al. (2012); (7) Vergani et al. (2011).

(Vergani et al. 2015), we restricted ourselves to the $z < 1$ range. To study the emission line properties of the host galaxies, we collected archival spectral observations of the hosts and carried out dedicated observational programmes to obtain the spectra of those hosts for which spectroscopic observations were lacking. In the following subsections we detail our final spectroscopic data sets grouped by the instrument with which they were obtained. For the sake of homogeneity we reduced and analysed the previously published data. In one case (GRB 080319B) we detected neither continuum nor emission lines. Our final sample therefore includes 13 host galaxies. The relevant information for each observation is summarized in Table 1.

2.1. VLT/X-Shooter

The X-Shooter spectrograph (Vernet et al. 2011) was used to observe eight hosts. For the purpose of this study we observed the GRB 081007 host (programme ID 095.D-0560, PI: S. D. Vergani). We also collected archival spectra of the hosts corresponding to GRBs 050416A, 050525A, 061021 (PI: D. Malesani), 060912A, 091018, 091127 (PI: J. P. U. Fynbo), and 100621A (PI: T. Krühler). All observations were performed using the nodding technique with an offset of 5″ between individual exposures. Each observation included a telluric star, whose spectrum was taken immediately before or after the host's and at a similar airmass. A spectrum of a spectrophotometric standard star was taken at the beginning or end of the night.

We processed the spectra using version 2.0 of the X-Shooter data reduction pipeline (Goldoni et al. 2006; Modigliani et al. 2010). The raw frames were first bias subtracted and cosmic-ray hits were located and removed following the method of van Dokkum (2001). The frames were divided by a master flat field. Day-time calibration frames were used to obtain a spatial-wavelength solution, necessary for the extraction and the rectification of orders. The rectified orders were shifted for the offset used in the observation and co-added to obtain a final two-dimensional spectrum, from which a one-dimensional spectrum with the corresponding error spectrum and bad-pixel map at the position of the source were extracted. In this way we reduced all observations, that is, those of the host galaxies, telluric stars, and spectrophotometric standards. Spectra of the latter were compared to tabulated flux-calibrated spectra (Vernet et al. 2010) to determine the response function, which was then applied to the spectra of the hosts and telluric stars.

2.2. VLT/FORS1 and FORS2

From the ESO archive we collected the data of the hosts observed with the FORS1 and FORS2 instruments. To our knowledge the spectrum of the host of GRB 060614 (FORS1; PI: J. Hjorth, programme ID 177.A-0591(H)) has not been previously published. Already published data include hosts of GRBs 060614 and 081007 (FORS2; PI: M. Della Valle), 071112C, 080916A (PI: P. Vreeswijk), and 090424 (PI: E. Pian).

The data were reduced using standard procedures for bias subtraction and flat-field correction. The extraction of the spectrum was performed with the ESO-MIDAS[2] software package. Wavelength and flux calibration of the spectra were achieved using a He-Ar lamp and observing spectrophotometric stars.

2.3. GTC/OSIRIS

We obtained GTC data with OSIRIS for the host galaxies of GRB 080430 and GRB 080319B (programme GTC31-13B;

[2] http://www.eso.org/projects/esomidas/

PI: A. Fernandez-Soto). The former were collected on January 7, 2014 and the latter over two nights on February 25 and 27, 2014. In both cases the observing strategy was the same: a brighter star was used as pivot and the target was centred on the slit by fixing the OSIRIS rotation angle. A total of 6600 s (divided into 8 × 825 s exposures) was integrated in each case, using a 15 arcsec dithering motion along the slit between each consecutive exposure. Conditions were good, with clear dark sky, and seeing ranging between 0.8 and 1.2 arcsec in different exposures. In addition to GRB 080430 and 080319B hosts, we collected observations of GRB 090424 (PI: A. J. Castro-Tirado) from the archive.

The data were reduced using standard procedures and calibration files as provided by the GTC. Wavelength calibration was obtained through the use of Hg-Ar, Ne, and Xe lamps that were observed during the same nights. A basic flux calibration was obtained using the spectrum of the pivot stars and multiband photometry from SDSS.

2.4. Flux calibration verification

Good flux calibration is essential to obtain reliable measurements of emission line fluxes. Flux-calibrated host spectra were compared and cross-calibrated to photometric observations of the hosts (Vergani et al. 2015). In this way the slit losses were taken into account. However, there were a few exceptions.

The host of GRB 050525A has no detectable continuum and therefore we could not use the magnitudes to check the flux calibration. The X-Shooter observations of telluric stars were obtained in similar conditions (airmass, seeing) and the same instrumental setup (binning, slit width) as the observations of scientific targets (e.g. hosts). We reduced the telluric star observation corresponding to the GRB 050525A host using the same instrumental response function as for the science observations to flux-calibrate the telluric star spectrum. Then we calculated the flux correction by comparing the telluric star flux-calibrated spectrum to photometric observations of the star. The same correction was applied to the host's spectrum. We note that we cross-checked this method for all other cases where both the host photometry and the telluric stars were available, and the flux corrections obtained in this way were consistent within ∼20% (see also Piranomonte et al. 2015 and Pita et al. 2014).

For GRBs 071112C, 091018, and 091127, the spectra are dominated by afterglow emission. Flux calibration was therefore cross-checked by using photometric afterglow observations at (or near) the epoch in which the spectra were taken. We used light curves published by Wiersema et al. (2012) and Filgas et al. (2011) for GRBs 091018 and 091127, respectively. For GRB 071112C, the joint data sets of Huang et al. (2012) and Covino et al. (2013) were used.

3. Analysis

Emission line fluxes were measured by fitting one or multiple Gaussian functions to the data, and they were cross-checked by integrating the signal below the line profile. Line fluxes (corrected for Galactic extinction, using extinction maps of Schlafly & Finkbeiner 2011 and the average Milky Way extinction curve of Cardelli et al. 1989) are reported in Table A.1. Errors for each line were estimated with a Monte Carlo simulation: for 1000 simulated events we repeatedly added random Gaussian noise (standard deviations were taken from the error spectra or rms of the continua) to the best-fit model and fitted the resulting spectrum by the same model. The obtained distribution of best-fit parameters was then used to compute the 1σ errors. In case of a non-detection we calculated 3σ upper limits by multiplying the rms in the region around the expected position of a line by 3. In cases where this resulted in particularly high upper-limits (e.g. GRB 050525A host), we additionally checked the values by adding an artificial line to the spectrum – assuming a Gaussian shape and *FWHM* as obtained from fitting strong lines of the same host – and trying to measure it. In all these cases the artificial lines were not significantly detected, therefore we trust the upper limits.

Neither continuum nor emission lines were detected in the GRB 080319B host. The Hα line was not covered by the GTC/OSIRIS spectrograph (see Table 1), while strong [O III] and Hβ fell in the region of strong telluric absorption. The host is faint (r(AB) ∼ 27; Tanvir et al. 2010), therefore it is expected that the continuum was not detected. In the following we leave the host of GRB 080319B out of the discussion, except when interpreting the effect that its absence has on the conclusions.

Balmer absorption lines are not clearly detected in our spectra, which is expected as LGRB hosts are faint young galaxies. The strength of the correction that should be applied to our measured line fluxes depends on several factors such as stellar mass and spectral resolution (e.g. Zahid et al. 2011). Even though our sample spectra come with a wide range of spectral resolutions, the correction in all cases can be roughly approximated by the equivalent width of 1 Å (Zahid et al. 2011; Cowie & Barger 2008), assuming the range of stellar masses of our sample (Vergani et al. 2015). The Balmer absorption correction is significant (i.e. larger than measured errors) only for the host of GRB 090424. For others, while the correction has been added to the measured values, it is usually smaller than the uncertainty even if we assumed much larger equivalent line correction (e.g. 2 Å).

3.1. Extinctions, metallicities, and star formation rates

The measured rest-frame extinctions, star-formation rates (SFR), and metallicities are reported in Table 2.

The host-integrated rest-frame extinctions A_V were determined from the Balmer decrement assuming gas with a temperature of $T = 10^4$ K (i.e. intrinsic ratios between different hydrogen Balmer lines are assumed to be Hα/Hβ = 2.87, Hγ/Hβ = 0.47 and Hδ/Hβ = 0.26; Osterbrock & Ferland 2006). To measure the extinctions we used only lines detected with 3σ confidence and assumed the Milky Way[3] extinction curve (Pei 1992). However, the hosts of GRB 050525A and GRB 080916A lack the Balmer lines needed to measure the extinction. While the line-of-sight extinction, measured from the afterglow spectral energy distribution, is available for the two cases, in general line-of-sight and host-integrated extinctions are not necessarily the same (e.g. see Sect. 5.3 and Perley et al. 2013). Therefore we assumed $A_V = 0$ in the case of these two hosts in the further analysis.

All the steps described in the following paragraphs were performed after applying the host extinction correction to the emission lines.

To measure the SFR, we used the Hα line where possible because it is the most reliable tracer of SFR and does not depend strongly on the uncertainties in the measured extinction. We assumed the conversion between Hα luminosity and SFR as

[3] We chose the Milky Way extinction curve because it is commonly used in the literature. We note that applying other commonly used extinction curves (e.g. Japelj et al. 2015) does not result in a significant difference in the measurement of A_V and the subsequent correction of line fluxes.

Table 2. Measured redshift, host extinctions, metallicites, and star formation rates of our sample.

GRB	z	$\log M_\star$	$A_V{}^a$	$12+\log\left(\frac{O}{H}\right)$		SFR	SF-tracer
		$M_\odot$	(mag)	M08	KK04	($M_\odot$ yr^{-1})	
050416A	0.6542	$9.17^{+0.12}_{-0.12}$	$1.77^{+0.61}_{-0.56}$	$8.50^{+0.15}_{-0.15}$	8.4 ± 0.2	3.45 ± 1.42	Hα
050525A†	0.6063	$8.1^{+0.6}_{-0.6}$	–	–	–	>0.10	[O III]
060614A	0.125	$8.09^{+0.13}_{-0.17}$	$0.65^{+0.51}_{-0.34}$	$8.46^{+0.20}_{-0.20}$	8.4 ± 0.2	0.007 ± -0.003	Hα
060912A	0.9362	$9.23^{+0.06}_{-0.07}$	$0.50^{+0.25}_{-0.25}$	$8.60^{+0.12}_{-0.12}$	$8.72^{+0.05}_{-0.08}$	5.07 ± 0.93	Hα
061021	0.3453	$8.5^{+0.5}_{-0.5}$	$0.32^{+0.38}_{-0.32}$	$8.48^{+0.20}_{-0.26}$	8.4 ± 0.2	0.04 ± 0.01	Hα
071112C	0.821	$8.89^{+0.15}_{-0.18}$	<0.2	$7.90^{+0.50}_{-0.35}$	$7.88^{+0.27}_{-0.17}$	1.1 ± 0.4	Hγ^b
080430	0.767	$8.15^{+0.12}_{-0.15}$	<0.1	$7.60^{+0.35}_{-0.35}$	$7.94^{+0.25}_{-0.21}$	1.65 ± 0.63	Hβ^b
080916A†	0.688	$8.98^{+0.07}_{-0.08}$	–	$8.44^{+0.38}_{-0.22}$	$8.00^{+0.32}_{-0.20}/8.99^{+0.17}_{-0.41}$	>0.20	[O II]
081007	0.5294	$8.78^{+0.47}_{-0.45}$	$0.49^{+0.37}_{-0.30}$	$8.32^{+0.20}_{-0.25}$	$8.32^{+0.10}_{-0.10}/8.58^{+0.10}_{-0.13}$	0.36 ± 0.07	Hα
090424	0.5445	$9.38^{+0.17}_{-0.19}$	$1.42^{+0.54}_{-0.51}$	$8.88^{+0.12}_{-0.20}$	$8.39^{+0.12}_{-0.13}/8.69^{+0.15}_{-0.13}$	2.88 ± 1.14	Hα
091018	0.9710	$9.52^{+0.08}_{-0.10}$	$1.25^{+0.75}_{-0.75}$	$8.48^{+0.22}_{-0.30}$	8.4 ± 0.2	2.98 ± 1.81	Hα
091127	0.4904	$8.67^{+0.07}_{-0.07}$	<0.3	$8.50^{+0.15}_{-0.15}$	$8.47^{+0.12}_{-0.11}$	0.25 ± 0.02	Hα
100621A	0.5426	$9.04^{+0.06}_{-0.05}$	$0.34^{+0.21}_{-0.18}$	$8.40^{+0.15}_{-0.20}$	$8.25^{+0.16}_{-0.14}/8.67^{+0.14}_{-0.20}$	8.92 ± 1.44	Hα

Notes. Stellar masses are adopted from Vergani et al. (2015). $^{(a)}$ Extinction was measured from the Balmer decrement for all cases but GRBs 050525A and 080916A – see text for details. $^{(b)}$ Flux of the significantly detected Balmer line was first transformed to the Hα flux (see text and Osterbrock & Ferland 2006) and then to the SFR. $^{(\dagger)}$ Because we lack the Balmer emission lines, the host extinction cannot be computed. Reported star-formation rates are therefore formally lower limits.

given by Kennicutt (1998), but scaled to the Chabrier (2003) initial mass function. In two cases (hosts of GRBs 071112C and 080430) we scaled other significantly detected (and extinction-corrected) Balmer lines to Hα (assuming intrinsic ratios between Balmer lines) and used the same prescription to derive the SFRs. None of the Balmer lines is significantly detected in the GRB 080916A and 050525A hosts, therefore we used the [O II] and [O III]λ5007 lines as SFR tracers for the two hosts, respectively. [O II] luminosity is known to be strongly correlated with SFR in the LGRB host samples (Savaglio et al. 2009; Krühler et al. 2015). Krühler et al. (2015) also found a correlation between L([O III]λ5007) and SFR, although the relation is quite scattered (the scatter of the relations was taken into account in the final estimation of the errors). We cross-checked the SFR-L([O II]) and SFR-L([O III]λ5007) relations found by Krühler et al. (2015) on our sample, using nine GRB hosts with simultaneously detected Hα, [O II], and [O III]λ5007 lines. We found nearly the same relations (and therefore almost identical calculated SFRs for the GRB 080916A and 050525A hosts), but with a slightly larger scatter. We also verified that the marginally detected Hα line of GRB 050525A gives a nearly identical value of SFR as [O III]λ5007. Because host extinction for the hosts of GRB 080916A and GRB 050525A is unknown, the measured SFRs are formally lower limits.

Gas phase metallicities of distant galaxies are typically measured using strong emission line ratios, whose dependence on metallicity has been determined either through theoretical models or through cross-calibration with direct metallicity measurements in the local Universe (e.g. see review by Kewley & Ellison 2008). We decided to measure metallicities by using the method of Maiolino et al. (2008; see also Mannucci et al. 2011), where gas-phase metallicities were computed by simultaneously minimising all metallicity indicators that can be used for each specific case. In principle, the method has two free parameters: host extinction and metallicity. However, since most of the indicators are built from ratios of lines of similar wavelengths, they are not sensitive to extinction, and therefore this parameter is largely unconstrained in the minimisation procedure. We therefore fixed the extinction values as obtained from the Balmer line ratios. We determined the metallicities for all cases but GRB 050525A. Even though we lack the host extinction measurement for the host of GRB 080916A, we do not expect it to have a significant effect on the metallicity measurement and the final conclusions (given the high metallicity errors measured in this case), unless extinction turned out to be very high ($A_V > 3$ mag). Such a high value of host average-extinction at $z < 1$ is very unlikely (see Fig. 11 in Perley et al. 2013). To prove that our conclusions do not depend on the choice of the assumed indicator, we also determined metallicities[4] using the R_{23}-based calibration of Kobulnicky & Kewley (2004; hereafter KK04). The calibration suffers from degeneracy, that is, for each measured line ratio we obtain two metallicity solutions. The degeneracy can be broken with the help of metallicity-dependent [N II]/[O II] or [N II]/Hα ratios. Several cases of our hosts have the KK04 metallicities near the turnover point at $12+\log\left(\frac{O}{H}\right)_{KK04} \sim 8.4$, and for these we assumed the metallicity of 8.4 and added an error of 0.2 dex. The metallicity solution for the hosts of GRBs 071112C and 080430 was also double valued with two extreme lower- and upper-branch values ($12+\log\left(\frac{O}{H}\right) = 7.88$, 8.91 and 7.94, 8.87, respectively). For both hosts we detect the [Ne III] emission line. The [Ne III]/[O II] diagnostic (Maiolino et al. 2008) clearly points to a low metallicity for both hosts ($12+\log\left(\frac{O}{H}\right) = 7.90$ and 7.50, respectively). We therefore chose the lower branch solution for these two galaxies. We note that the reliability of diagnostics that are based on [O III] and [N II] emission lines at high redshifts have been questioned (Kewley et al. 2013; Shapley et al. 2015). However, this uncertainty is not expected to affect our $z < 1$ sample study.

[4] We also used the pyMCZ software (Bianco et al. 2015).

4. Comparison star-forming galaxy samples

We wish to compare the SFR and metallicity properties of our LGRB host galaxy sample with sample(s) of a field population of star-forming galaxies. To make the comparison reliable, spectroscopic surveys are necessary. In addition, the completeness limits of the surveys (in terms of brightness, SFRs, and stellar masses) need to be deep enough for a valid comparison with our BAT6 sample. It is difficult to find surveys with such characteristics. The best survey is the VIMOS VLT Deep Survey (VVDS; Le Fèvre et al. 2005), especially because its magnitude selection is deep enough to cover the faint magnitudes of the hosts in our sample. We adopted the VVDS sample as the primary comparison sample. As explained in detail in the following, a few other surveys were also used for different tests.

In the following, all the stellar masses were scaled to the Chabrier (2003) IMF.

4.1. VIMOS VLT Deep Survey

The VVDS is a comprehensive survey of $z < 6.7$ star-forming galaxies conducted with the VLT/VIMOS multi-object spectrograph (Le Fèvre et al. 2003). We retrieved the last data release (Le Fèvre et al. 2013) from the VVDS-database[5]. In particular, we selected the data corresponding to $0.1 < z < 1.0$ star-forming galaxies collected in magnitude-limited Deep ($17.5 \leq i_{\rm AB} \leq 24$) and Ultra-Deep ($23 \leq i_{\rm AB} \leq 24.75$) surveys. The latter covers an area on the sky included in the former field. The combined sample consists of a total of 6366 galaxies with measured stellar masses and host extinction. From this sample, we selected galaxies with detected emission lines. In particular, for the purpose of calculating the emission-line-based SFR, we required a detection of at least one of the following lines: [O II], Hα, or Hβ with significance $>2\sigma$. This requirement reduced the number of galaxies in VVDS sample to 3551. The properties of this sample (i.e. distributions of apparent $i_{\rm AB}$ and absolute $M_{\rm B}$ magnitudes, stellar masses, and redshift) do not differ significantly from the original sample, therefore, we did not introduce any additional bias with these selection requirements (see Fig. A.1).

Star formation rates were calculated in the following way. Line fluxes were corrected for host extinction. Following our procedure for BAT6 hosts, we calculated SFRs from the Hα or Hβ line. If neither of the two was available (or was detected with a very high uncertainty), [O II] was used to measure the SFR. In the latter case, we used the calibration between SFR, [O II] luminosity, and intrinsic brightness $M_{\rm B}$ of the hosts given by Moustakas et al. (2006). After the SFRs were obtained, we compared the sample properties to some of the other samples to cross-check whether our selection is unbiased and to better understand the completeness limits[6]. We found that the SFR-weighted mass distribution of the SFR-selected VVDS sample agrees very well with the UltraVista sample (Ilbert et al. 2013) used by Vergani et al. (2015) as a reference sample of masses of field galaxies. Second, the SFR-weighted SFR distribution agrees quite well with the SFR-weighted distribution built from the Hα luminosity function of Ly et al. (2011; hereafter Ly11, see Fig. 1 and Sect. 3.2.2). The SFR completeness limit of the VVDS and Ly11 surveys is similar with $\log SFR\,[M_\odot\,{\rm yr}^{-1}] \sim 0.0$.

We determined metallicities using two different methods. First, we used the same approach as for the BAT6 hosts, that is, we simultaneously minimised a number of different line ratios corresponding to different calibrators. Unfortunately, only a portion of the VVDS sample has enough emission lines detected to provide a reliable metallicity determination (if other indicators are used this portion is even smaller). Upon examination we found that the subsample for which we were able to measure the metallicity was slightly biased towards low stellar masses and therefore low metallicities. As the VVDS galaxies represent a field population of star-forming galaxies, they should follow the fundamental mass metallicity relation (FMR; Mannucci et al. 2010, 2011). Using the stellar masses and the previously measured SFRs for the SFR-selected VVDS sample, we can therefore calculate the metallicities from the FMR[7]. As expected, the metallicites calculated from the two methods do not differ statistically for the aforementioned subsample. In the following we therefore use the FMR-based metallicities.

4.2. NEWFIRM Hα survey

The majority of the SFRs determined for the VVDS sample is based on the luminosity of the [O II] line, for which the strength of the line is sensitive to the abundance and ionization state of the gas (Kewley et al. 2004), making the [O II]-SFR relation rather controversial (e.g. Moustakas et al. 2006 and references within), especially for heterogeneous samples of galaxies. We therefore additionally used the NEWFIRM Hα survey of star-forming galaxies Ly11 for the purpose of comparing the SFR distributions of LGRB hosts and star-forming population.

The Ly11 field galaxy SFR distribution is the result of the NEWFIRM narrowband Hα observational campaign. By observing a sample of ~400 star-forming galaxies at $z \sim 0.8$, Ly11 built an Hα luminosity function at this redshift. For the comparison with the LGRB host galaxies, we multiplied the Ly11 luminosity function (described by a Schechter function with $\log(L_*/({\rm erg\,s^{-1}})) = 43.00$ and $\alpha = -1.6$) by the luminosity to account for the assumption that the probability of hosting an LGRB is proportional to the SFR of a galaxy. Luminosities were then converted into SFRs (following Kennicutt 1998; but scaled to Chabrier 2003 IMF).

4.3. Other star-forming galaxy samples

Most of the LGRB host galaxies in our $z < 1$ sample have stellar masses below $10^9\,M_\odot$ and quite high specific SFR (see Sect. 5.1.1). We therefore also considered for comparison samples focused on these types of star-forming galaxies to see whether they have similar properties as LGRB host galaxies. We note that the following two samples are biased because they were both selected to address specific star-forming populations.

Atek et al. (2014) presented the properties (stellar masses and SFRs) of 1034 galaxies at $0.3 < z < 2.3$ selected through emission lines with the WISP (Atek et al. 2010) and 3DHST (Brammer et al. 2012) surveys. This selection favours the detection of starburst galaxies. We used the $0.3 < z < 1$ subsample

[5] http://cesam.lam.fr/vvdspub/

[6] When comparing cumulative distributions, we compare LGRB host properties (e.g. SFR or metallicity) with SFR-weighted properties of field star-forming galaxies. We therefore assume that the probability of hosting an LGRB is proportional to the SFR of a galaxy. If the properties of the two populations differed, then the initial assumption that we tested was incorrect, and we tried to understand the factors that made it so.

[7] In the calculation of the FMR-based metallicity we account for errors in measured SFR and stellar mass as well as intrinsic dispersion of the FMR relation (~0.06 dex). The effect of the latter is negligible.

properties for comparison with those of the LGRB host galaxies in our sample (see Sect. 5.1.1).

We also used the sample of 45 low-mass star-forming galaxies and 29 blue compact dwarf galaxies (BCD, defined following Gil de Paz et al. 2003) studied by Rodríguez-Muñoz et al. (2015) to check if the GRB host galaxies have in some way properties similar to these classes of galaxies. These samples have been selected at first using photometry but then a spectroscopic redshift determination is required, hence implying the detection of emission lines.

5. Results and discussion

5.1. Star formation rates and stellar masses

5.1.1. Star formation rates

The cumulative SFR distribution of our 13 LGRB hosts (Table 2) is shown in Fig. 1. Because of the uncertainty in the estimated host extinction, the SFR errors are quite high in some cases. For this reason we also plot the 1σ uncertainty region (shaded), obtained by performing MC simulation in which the distributions are generated from the SFRs, varied by the measured error. In the same plot we show the SFR-weighted cumulative distributions of the VVDS and Ly11 samples. As illustrated in Fig. 1, LGRB hosts can hardly be drawn from the star-formation weighted distribution of star-forming galaxies. The average redshifts of the BAT6, VVDS, and Ly11 samples are $\langle z \rangle = 0.62, 0.7$ and 0.8, respectively. The SFR density of field galaxies is observed to evolve with redshift (e.g. Whitaker et al. 2012; Speagle et al. 2014). To remove a systematic difference that is due to the effect of the observed evolution, we cut the BAT6 sample including only $0.5 < z < 1$ hosts (excluding lower limits, this leaves us with a sample of eight hosts) with $\langle z \rangle = 0.72$. It is evident from Fig. 1 that in this way we cut the low end of the SFR distribution.

To quantify the difference between the two samples, we performed a Kolmogorov-Smirnov (KS) test that shows whether the BAT6 (cut sample, where lower limits are not taken into account) and Ly11 samples[8] are drawn from the same distribution. We ran a MC simulation, in which we randomly chose SFRs from BAT6 sample (varying the measured values by their errors) and a number of 400 SFR values (number of galaxies in Ly11 sample), randomly chosen from the Ly11 distribution (Fig. 1). This resulted in a probability of $p \approx 0.007$, which suggests that we can discard the hypothesis. This test was performed considering the Ly11 luminosity function only in the range in which the completeness limit of the Ly11 sample is trustworthy (i.e. down to H$\alpha = 10^{41}$ erg cm^{-2} s^{-1}, which corresponds to log $SFR[M_\odot\,\mathrm{yr}^{-1}] \sim 0$). However, as seen in Fig. 1, the SFRs of the BAT6 sample extend to lower values. To account for this discrepancy, we made two additional tests. First we cut the BAT6 sample to the same SFR completeness limit, resulting in a probability of $p \approx 0.015$. Alternatively, we assumed that the Hα luminosity function can be simply extrapolated to lower luminosities[9] (down to H$\alpha = 10^{40.3}$ erg cm^{-2} s^{-1} to match the lowest value of our cut BAT6 sample; dotted line in Fig. 1). Using the extrapolated distribution, the KS test gives values of $p \approx 0.02$. We therefore conclude that LGRB formation is more efficient in a low SFR environment (see also the similar comparison and results found by Krühler et al. 2015 for their X-Shooter sample of GRB host galaxies).

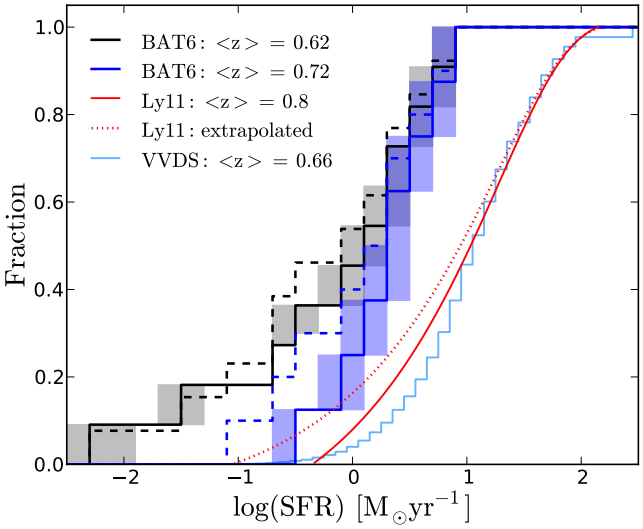

Fig. 1. Cumulative SFR distributions of our sample (solid black line) and its $z > 0.5$ subsample (solid blue line). Shaded regions show the 1σ sampling range around solid lines. Dashed lines show distributions including lower limits. For comparison we also plot a star-formation-weighted distribution of $z = 0.8$ star-forming galaxies (Ly et al. 2011) (red solid line), the same distribution extrapolated towards lower SFRs to account for the completeness limit of the survey (red dotted line), and the $z > 0.3$ VVDS sample (light blue line; see text for details).

5.1.2. SFR vs. stellar mass relation

A correlation between the SFR and the stellar mass, known as the star formation main sequence (SFMS), has been found to exist for star-forming galaxies in the full range from low ($z < 1$; Brinchmann et al. 2004) to high ($z \sim 6$; Steinhardt et al. 2014) redshifts. Both the slope and normalisation of the correlation are observed to change over cosmic time (e.g. Speagle et al. 2014). To asses whether GRB hosts occupy the same *SFR*-$M_\star$ region as the field star-forming galaxy population, we plot our BAT6 sample in the *SFR*-$M_\star$ plane (Fig. 2a). We compare our values to the star-forming galaxies from the VVDS survey.

In general, the SFR of the BAT6 sample increases with stellar mass, as expected. In agreement with the results of Paper I, there is a clear discrepancy on the stellar mass range covered by the VVDS and the LGRB host galaxies, the first extending to much higher stellar masses. Within the LGRB stellar mass range, while the values for GRB hosts are quite scattered, they occupy the same region as VVDS field galaxies (at similar redshifts). Two low-redshift hosts (corresponding to GRBs 060614A and 061021) stand out with very low values of both SFR and specific SFR. We caution, however, that GRB 060614A is rather peculiar in itself, because even though its duration clearly makes it a long GRB, no supernova (SN) has been detected at the position of the burst, despite its near origin and a comprehensive follow-up campaign (Fynbo et al. 2006; Della Valle et al. 2006). Recently re-analysed late-time data of this GRB afterglow show evidence (Yang et al. 2015; Jin et al. 2015) of an emerging macronova emission (Li & Paczyński 1998), the radioactive decay of debris

[8] It does not affect the conclusions whether we compare our results with the VVDS or Ly11 samples.

[9] The cumulative distribution depends on the assumed SFR limit, meaning that it will change if we extrapolate the distribution down to lower SFRs. Our conclusion is therefore sensitive to the assumed limit. However, even if we extrapolate the luminosity function down to log $SFR[M_\odot\,\mathrm{yr}^{-1}] = -2$, the cumulative distribution does not change much and the significance of the discrepancy remains similar. This is because the distribution is weighted for SFR.

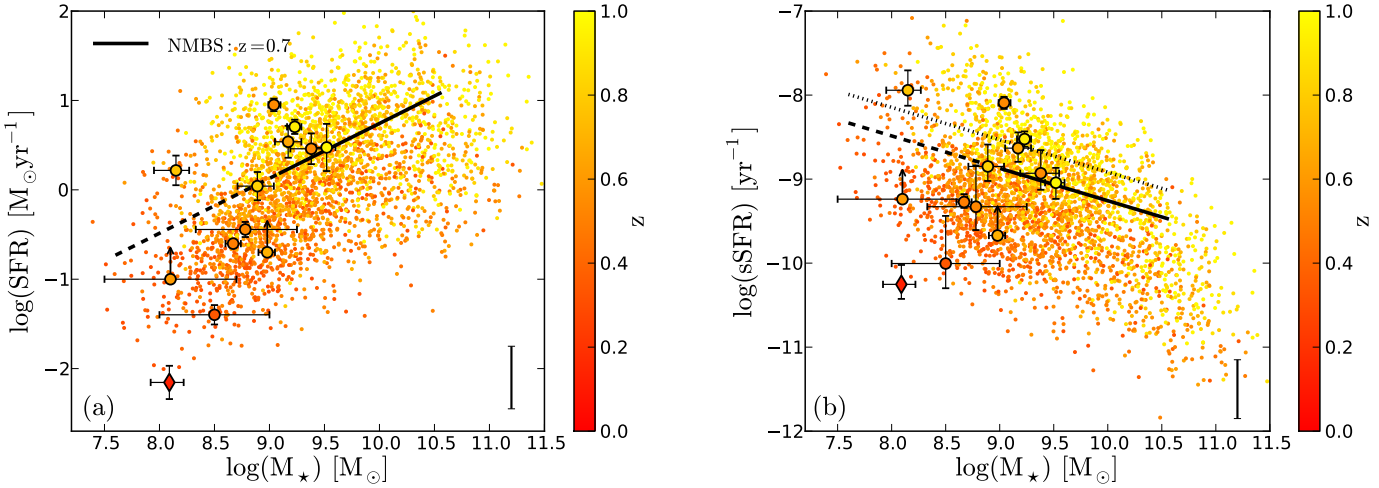

Fig. 2. a) SFR-stellar mass relation for BAT6 sample. The host of the GRB 060614A is plotted with a different symbol (diamond) to emphasise the dubious nature of the GRB. The colour-coding corresponds to redshifts as noted with the colour bar on the right sight of the plot. Small points with the same colour-coding correspond to the $0.3 < z < 1.0$ VVDS survey of star-forming galaxies (Le Fèvre et al. 2013). In addition, we plot the median value of SFR-stellar mass relation at $z \sim 0.7$ (mean redshift of the VVDS sample and the BAT6 sample without the host of GRB 060614) as observed in the NEWFIRM medium band survey (NMBS; Whitaker et al. 2012). We note that the latter relation has a scatter of ±0.34 dex (indicated by an error bar in the plots). With a dashed line we draw the extrapolation of the relation below the stellar mass completeness of the Whitaker et al. (2012) survey. **b)** Specific SFR-mass relation. The median value of the Whitaker et al. (2012) relation at $z \sim 0.7$ is plotted. The dotted line represents the relation plus the dispersion (0.34 dex).

following a compact binary merger. The origin of this GRB is therefore most likely different from the other LGRBs in the sample. This does not affect our results because this GRB host is excluded from every comparison in the following as it fails to satisfy the completeness limits of the surveys.

5.1.3. Comparison with starbursts and BCD galaxies

We then compared the SFR and sSFR vs stellar mass trend with the $0.3 < z < 1$ star-forming galaxies studied by Atek et al. (2014) and the low-mass star-forming galaxies and BCDs studied in Rodríguez-Muñoz et al. (2015) (see Sect. 4.3). GRB host galaxies have on average higher stellar masses than BCDs. We cannot compare the stellar masses with low-mass star-forming galaxies of Rodríguez-Muñoz et al. (2015) because they were originally selected to have stellar masses lower than $10^8\,M_\odot$, that is, the mass region that is not covered by our BAT6 sample. In the common covered range of stellar masses, SFR and sSFR show a large but similar spread. The selection of the Atek et al. (2014) sample was based on emission line detections, therefore its SFR limit ($\log\ SFR[M_\odot\,\mathrm{yr}^{-1}] \sim -1$) needs to be taken into account when comparing it with our LGRB host galaxy sample. Within the SFR limits of the Atek et al. (2014) surveys (therefore excluding the host galaxies of GRB 060614 and GRB 061021), GRB host galaxies occupy a smaller stellar mass range and have similar SFR.

Since the Atek et al. (2014) survey specifically selected galaxies with high specific star-formation rates, we became interested in the percentage of starbursts in the LGRB hosts and the galaxy sample of Atek et al. (2014) and field sample (VVDS) in the $0.5 < z < 1.0$ redshift range – the average redshift of each of the three populations in this range is $z \sim 0.7$. Whitaker et al. (2012) studied a sample of $0 < z < 2.5$ star-forming galaxies and found that the SFR-$M_\star$ relation of their sample had a scatter of ±0.34 around the median relation and that the scatter was independent of stellar mass and redshift. The median relation (Eq. (1) in Whitaker et al. 2012) at $z = 0.7$ is plotted in Figs. 2 and 3. Following their result, we calculated how many galaxies of a given population have a specific star-formation rate above the star-formation sequence (e.g. above the dotted line indicating the +0.34 dex scatter; see Figs. 2b and 3b). We found that 27 (−9,+15)%, 27%, and 17% of galaxies are categorised as starbursts (according to our prescription) for the LGRB hosts, the sample of Atek et al. (2014), and the VVDS field sample, respectively[10]. This result is in line with our expectations. Because the GRB formation probability scales in some way with the SFR, we expect a higher incidence of starburst galaxies in GRB-selected samples than in those of field galaxies. It would be interesting to perform a similar analysis and compare the SSFR cumulative distributions taking the completeness limits of the survey into account. Unfortunately, we lack the statistics because our sample will be reduced to six objects only, which is not suitable for reliable results.

5.2. Metallicities

5.2.1. Mass-metallicity relation

In Fig. 4 we plot the *MZ* relation of the BAT6 sample both in the (a) M08 and (b) KK04 metallicity calibration.

We compared our values with the *MZ* relation of field galaxies, taking the evolution of the relation with redshift into account (e.g. Savaglio et al. 2005; Mannucci et al. 2009; Zahid et al. 2013a). When we exclude the host of troublesome GRB 060614, the redshift range of our sample is $0.3 < z < 1$ and the average redshift is ~0.7. Therefore we compared our sample to the median value of *MZ* relation at this redshift bin. The paucity of LGRB host galaxies at super-solar metallicity is evident.

[10] Whitaker et al. (2014) extended the analysis to lower stellar masses. However, their analysis prevented them from studying the scatter around the median relation, therefore we cannot use their findings for the present study. We note that, assuming the median SFR-$M_\star$ relation by Whitaker et al. (2014) and a constant scatter of ±0.34, the fractions of starbursts do not change significantly.

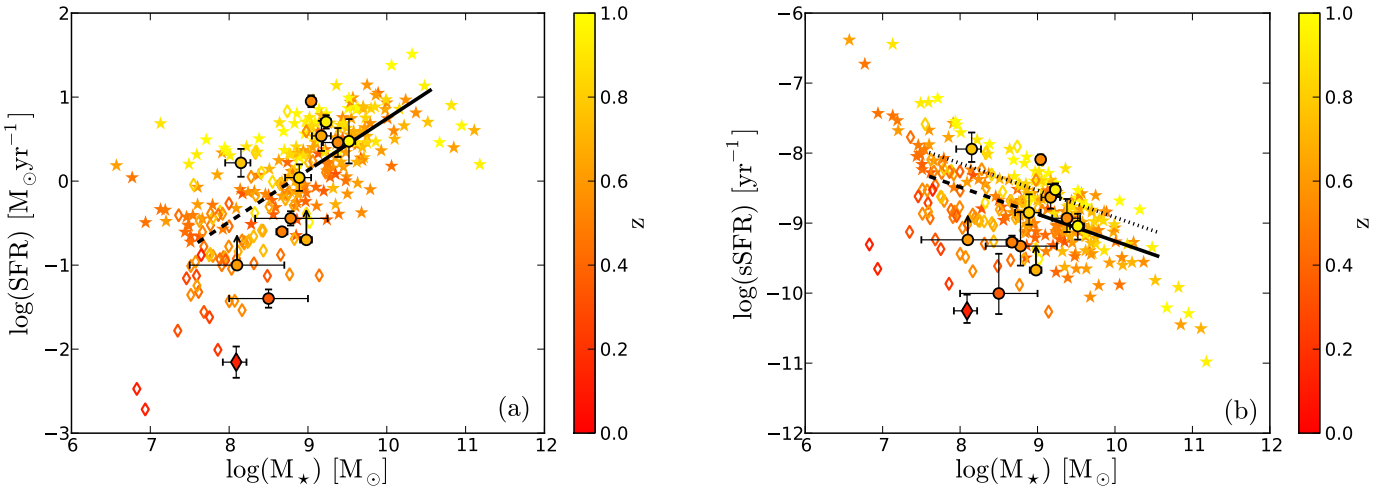

Fig. 3. Comparison of **a)** SFR-stellar mass and **b)** sSFR-stellar mass relations of our BAT6 sample to the samples of extreme starbursts (star symbols; Atek et al. 2014) and blue compact dwarf galaxies (empty diamonds; Rodríguez-Muñoz et al. 2015). The colour scale and the overplotted lines are the same as in Fig. 2. The host galaxies of GRB 060614A and 061021, while included in the plots, were excluded from the comparison of specific SFRs (see text) because their measured SFR is below the completeness limit of the two surveys (log $SFR[M_\odot\,\mathrm{yr}^{-1}] \sim -1$).

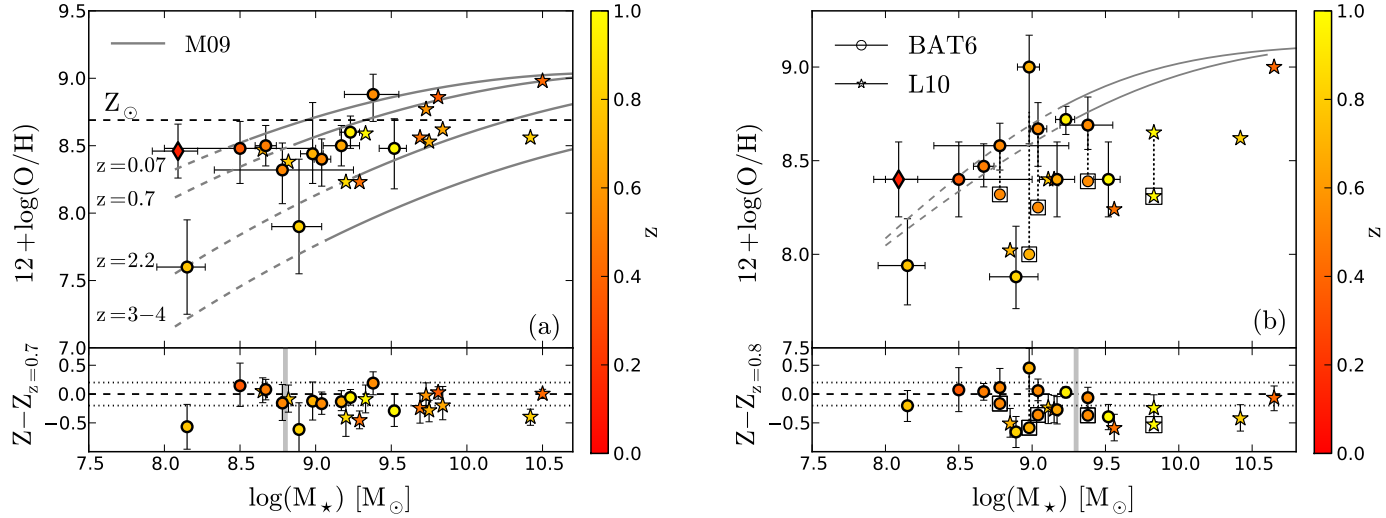

Fig. 4. Comparison of the BAT6 sample hosts (circles) to the average mass-metallicity relations at different redshifts. **a)** Metallicities are presented in the Maiolino et al. (2008) calibration. Overplotted are the models fitted to star-forming galaxy populations at different mean redshifts in the range of $z \sim 0.07$–4 (M09; Mannucci et al. 2009). As a comparison sample (stars) we plot the incomplete sample compiled by Mannucci et al. (2011) over $0.3 < z < 1$. **b)** Metallicities are presented in the Kobulnicky & Kewley (2004) calibration. Both upper and lower branch solution are plotted in cases where one solution cannot be obtained – in these cases the two values are connected with a dashed line and the lower branch solution is plotted within a square for clarity. For comparison we also include the incomplete sample of LGRB hosts from Levesque et al. (2010a) (stars) $0.3 < z < 1$. Lines represent fitted relations for galaxies at $z = 0.3$ and 0.8 (Zahid et al. 2013a). The extrapolation towards low stellar masses is indicated by dashed lines. *Lower panels* show the difference between the LGRB metallicities ($0.3 < z < 1$) and the median relations at redshift **a)** 0.7 and **b)** 0.8, respectively. Vertical grey lines in the *lower panels* mark the mass below which the two relations have been extrapolated. Errors of the comparison samples are not plotted in the *upper panels* for clarity, but are taken into account when calculating the difference from median relations (both errors in mass and metallicity are accounted for). The dotted horizontal lines in the *lower panels* show the intrinsic dispersion of the median relations – we assume a typical value of ±0.2 dex.

Accounting for errors, the fraction of hosts with metallicities above solar is found to be $16(-8,+16)\%$. For comparison, Krühler et al. (2015) retrieved the same result of $16 \pm 7\%$ for their sample of $z < 1$ hosts. At sub-solar metallicities, our sample appears fairly consistent with the *MZ* relation within the dispersion, and it does not show a systematic shift towards values below the relation found in some of the incomplete samples (see e.g. Fig. 4b and the sample of Levesque et al. 2010a). For four hosts we were unable to break the degeneracy of the KK04-based metallicity. If the lower-branch solution is assumed as the correct one for the four cases, then our sample seems to follow the *MZ* relation up to $\log M_\star[M_\odot] \sim 8.7$, after which it starts to deviate towards lower metallicities. In the latter case it behaves in a similar way as the sample from Levesque et al. (2010a) over the same redshift range. Regardless of interpretation, we note that the comparison of our sample with the star-forming *MZ* relation is subject to much uncertainty because many of our hosts have masses below the limits of *MZ* relation obtained with galaxy surveys. We simply extrapolated the polynomials fitted to the relations at higher masses, but this may deviate from the real conditions. We also briefly mention that similar conclusions as for the *MZ* relation can be found when considering the relation

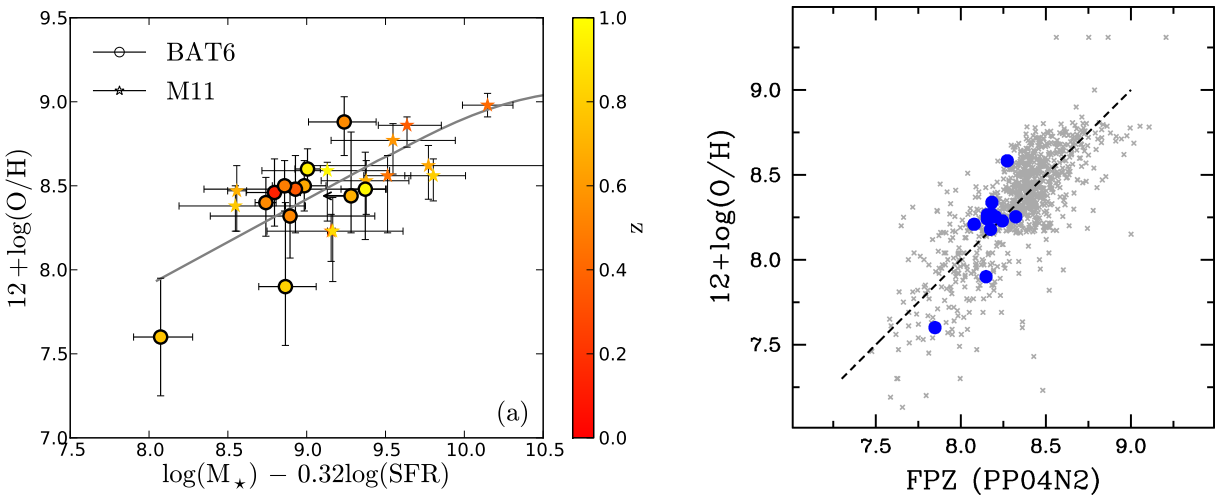

Fig. 5. **a)** Fundamental metallicity relation (Mannucci et al. 2010, 2011). Our sample (circles) is compared to the incomplete sample of Mannucci et al. (2011; stars). **b)** Fundamental metallicity plane (FPZ) for low-mass galaxies (Hunt et al. 2016). BAT6 sample (blue) is compared to different species of low-mass galaxies (grey). The plotted relation is done with [N II]/Hα metallicity calibration (N2; Pettini & Pagel 2004), and our data have been transformed to this calibration following Kewley & Ellison (2008).

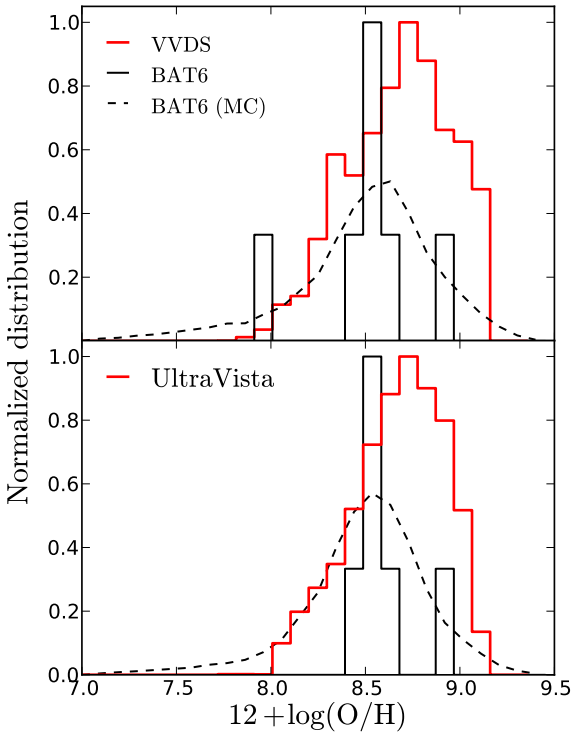

Fig. 6. Metallicity distribution of the BAT6 sample (solid black line) compared to the SFR-weighted distributions of VVDS and UltraVista samples of field galaxies (red lines). The dashed lines represent the average BAT6 distribution, obtained by taking the errors of the measured metallicities into account (through a MC simulation).

between gas-phase metallicity and stellar-to-gas mass ratio, as parametrised by Zahid et al. (2014). We show this in Fig. A.2.

It has been shown that star-forming galaxies (at least up to $z < 2.5$) follow a well-defined relation between stellar mass, SFR, and metallicity, known as the fundamental metallicity relation (FMR; Mannucci et al. 2010). We plot the FMR relation for GRB hosts in Fig. 5a. As found by Mannucci et al. (2011), LGRB host galaxies follow the FMR within errors, meaning that they are equally scattered around the relation even though with a quite large dispersion. Nevertheless, FMR is not well defined when approaching the low stellar masses that dominate in our sample. For example, Hunt et al. (2012) found that low-mass starburst galaxies deviate from the relation and that the mass-*SFR*-*Z* plane has to be recalibrated for such objects. We therefore also plot LGRB hosts in the recently calibrated relation (Hunt et al. 2016). As shown in Fig. 5b, LGRB hosts lie near the relation with a similar scatter as other low-mass galaxy samples.

5.2.2. Metallicity distribution

With the *MZ* relation we can examine whether the LGRB host population lies in the same plane as star-forming galaxies, but it does not give insight on the frequency with which LGRBs occur as a function of metallicity with respect to the star-forming population. Therefore we also compared the metallicity distribution of BAT6 hosts to VVDS and UltraVista (see Paper I) field galaxy samples (Fig. 6). For both surveys we calculated the metallicity using the FMR relation. Since it is based on the stellar mass and SFR of the galaxies, we applied a cut to our GRB host galaxy sample following the stellar mass and SFR limits of both surveys to make the comparison. For the VVDS, we selected events with $i(\mathrm{AB}) < 24.75$ and $\log SFR[M_\odot\,\mathrm{yr}^{-1}] > 0.0$, while for the UltraVista comparison the selection encompassed events with $K(\mathrm{AB}) < 24.0$ and $\log SFR[M_\odot\,\mathrm{yr}^{-1}] > 0.4$. The resulting BAT6 samples are therefore cut to a rather low number of six and seven events, respectively. We note that the BAT6 hosts without measured metallicities (hosts of GRBs 050525A and 080319B) and the host of peculiar GRB 060614 were automatically excluded from the comparison samples and therefore do not affect the conclusions. The comparison samples were furthermore limited to $z > 0.3$ because the two surveys are incomplete at $z \lesssim 0.3$ and because of the lack of GRB hosts in BAT6 sample in that redshift range.

The samples compared in Fig. 6 have similar average redshifts: both VVDS and UltraVista samples have $\langle z \rangle = 0.76$, while BAT6 samples have $\langle z \rangle = 0.74, 0.72$ in the top and bottom plot. We here examine a small sample of LGRB hosts,

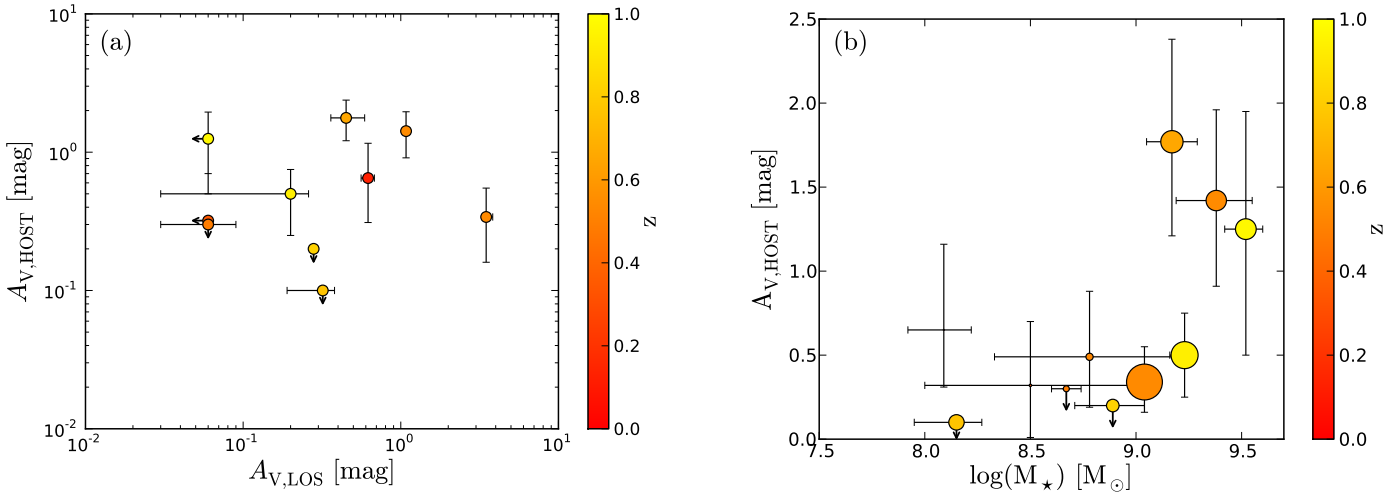

Fig. 7. a) Host-averaged extinction, measured from Balmer lines (e.g. Table 2) compared to line-of-sight extinction (Covino et al. 2013). Colour-coding corresponds to redshift. **b)** Observed relation between stellar mass and host-averaged extinction. Circle sizes for the hosts are proportional to the values of their star formation rates.

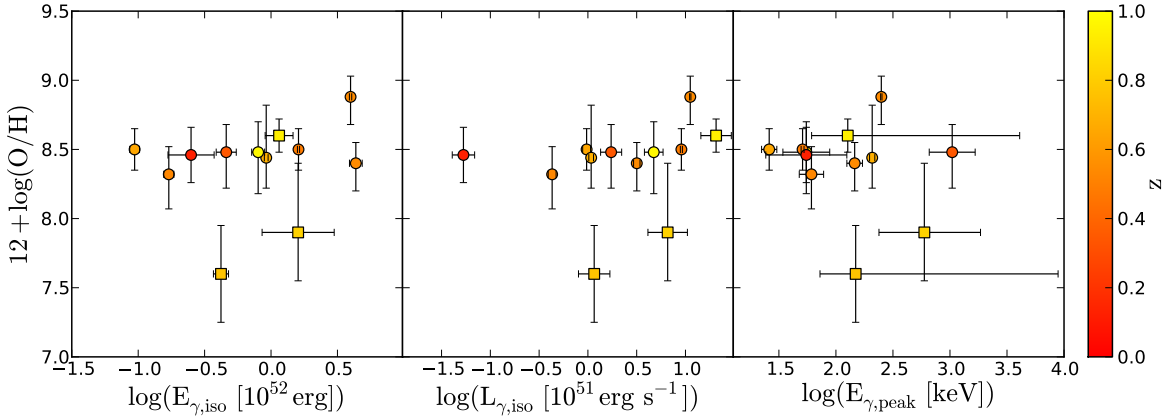

Fig. 8. Comparing high-energy properties of GRBs in the BAT sample and metallicities of their host galaxies. High-energy properties of events plotted with circles are taken from Nava et al. (2012). The three events plotted with squares have their peak energy (i.e. the peak in νF_ν spectrum) outside the energy coverage of the BAT instrument: we estimated the peak by using the correlation between $E_{\gamma,\mathrm{peak}}$ and spectral index Γ, found by Sakamoto et al. (2009), and then computed $E_{\gamma,\mathrm{iso}}$ and $L_{\gamma,\mathrm{iso}}$ in the extrapolated 1–10 000 keV range (e.g. Pescalli et al. 2016).

therefore we built a median distribution (dashed line) by taking errors into account and performed an MC simulation. Our comparisons to VVDS and UltraVista surveys, taking the completeness in brightness, SFR, and M_* of the samples into account, indicate that the metallicities of LGRB hosts and star-forming galaxies have similar distributions up to $12 + \log\left(\frac{\mathrm{O}}{\mathrm{H}}\right) \sim 8.4$–8.5, after which the already discussed paucity of high-metallicity hosts is observed. This cutoff value, obtained by direct comparison, is similar to the one found in an indirect way in complete-sample studies by Vergani et al. (2015) and Perley et al. (2016b). Finally, we note that there are two hosts with very low metallicities in the BAT6 sample with poorly constrained values, which limits their weight in the analysis. In addition, the small number of events used in the comparison prevents us from making quantitative, and therefore stronger, statistical conclusions.

5.3. Dust

Lastly we examine the dust properties of our host sample. We started by checking the relation between host-averaged extinction ($A_{V,HOST}$), measured from Balmer decrement (i.e. Table 2) and extinction in the GRB line of sight ($A_{V,LOS}$), measured from the SED analysis (Covino et al. 2013). Out of 14 events in the BAT6 sample, 10 cases have measurements (or estimated upper limits) of both quantities. Figure 7a reveals that the two quantities of our sample of hosts are not correlated. Perley et al. (2013) studied the same relation using a sample of GRBs extending to higher redshifts and higher line-of-sight extinctions. Their work focused on the class of dark bursts (e.g. Jakobsson et al. 2004). They showed that, approximately, the more extinct afterglows indeed tend to originate in dustier hosts. However, the relation is subject to considerable deviations of individual bursts from the $A_{V,HOST} = A_{V,LOS}$ correspondence and, especially for low $A_{V,LOS}$, to large dispersion. Furthermore, at redshifts $z < 1$ Perley et al. (2013) did not find any host with $A_{V,HOST}$ larger than the values in our sample. The lack of correlation for the $z < 1$ sample is thus consistent with previous studies.

It has been established that extinction in star-forming galaxies in general increases with stellar mass (e.g. Zahid et al. 2013b). We show in Fig. 7b that the trend is also observed in our sample, although admittedly our analysis includes galaxies from a wide redshift interval, in which the observed evolution of extinction with redshift could by itself introduce a bias into the relation.

5.4. High-energy properties

The BAT6 sample selection is based on the brightness of the prompt gamma-ray burst emission. To further verify the reliability of our results, we therefore checked for a correlation between the GRB energy output in γ-ray emission (E_γ) and its host metallicity. We looked for a relation between metallicities and high-energy properties, namely isotropic equivalent γ-ray energy $E_{\gamma,\rm iso}$, isotropic peak luminosity $L_{\gamma,\rm iso}$, and peak energy $E_{\gamma,\rm peak}$, for our BAT6 sample. We found no evidence for a correlation of these properties with metallicity. Similar conclusions have been also found by Levesque et al. (2010b). With the present evidence we can therefore assume that our results are not affected by our sample selection criteria.

6. Conclusions

We have presented a spectroscopic study of a sample of 14 $z < 1$ LGRB host galaxies drawn from the *Swift*/BAT6 complete sample of bright LGRBs. Our work compared derived host galaxy properties (SFR, metallicity, and stellar masses) to those of the general star-forming galaxy population and also investigated the relations between those properties.

We investigated the role of metallicity in the efficiency of LGRB production. Early studies (see Introduction) on the subject based on incomplete LGRB samples reported a strong preference towards low metallicity values. Lately, however, various studies have indirectly pointed out that this view is only partially correct (Vergani et al. 2015; Krühler et al. 2015; Perley et al. 2016b). Our results showed that at $0.3 < z < 1$ LGRBs preferentially select galaxies of sub-solar metallicities ($12 + \log\left(\frac{\rm O}{\rm H}\right) \sim$ 8.4–8.5) and therefore of low stellar masses. While the paucity of the super-solar metallicity hosts is striking, at sub-solar metallicities we find no evidence for a shift towards lower values on the *MZ* relation based on star-forming galaxies at similar redshift.

The preference for LGRBs to explode in sub-solar metallicity galaxies is very likely also the explanation of the observational evidence that LGRB hosts at $z < 1$ have on average lower star-formation rates than if they were direct star-formation tracers. Nevertheless, within the population of low-metallicity, low-mass, and low-SFR galaxies they seem to be preferentially selecting galaxies with high SFR, as shown by an increased fraction of starbursts (i.e. high specific SFR galaxies) among the LGRB host galaxies with respect to those of the field star-forming galaxy population. Unfortunately, our sample is too small (and the galaxy surveys not deep enough) to obtain a reliable result and to investigate in more detail whether the starburst fraction of host galaxy is the one expected under the hypothesis that GRBs are connected to SFR, after taking the high-metallicity aversion into account.

The preference for LGRBs to avoid high-metallicity galaxies can be related to the condition necessary for the progenitor star to produce an LGRB. Single-star progenitor models favour low metallicity, but some of them require very low metallicity cuts (Hirschi et al. 2005; Yoon et al. 2006) and cannot explain hosts with observed near-solar (or higher) metallicity. All resolved host galaxy observations have shown that LGRB host galaxies have almost negligible metallicity gradients (e.g. Christensen et al. 2008; Levesque et al. 2011). Assuming that this holds for all hosts, the discrepancy between the expected low-metallicity cut and observed near-solar metallicity therefore cannot be explained by the difference between the metallicity at the explosion site and the measured host-averaged metallicity. Furthermore, Modjaz et al. (2008) found that broad-line core-collapse SNe accompanying LGRBs are found in less metal-rich environments than those without detected GRBs, with a metallicity threshold similar to the one found in this study. This result shows that the two types of transients preferentially occur in different conditions and suggests different progenitor properties. There is more and more evidence that binary stars represent a significant fraction of core-collapse SN progenitors. Even if to a lesser extent, metallicity can also influence the evolution of binary stars (Belczynski, priv. comm.). It will be interesting in the future to compare our results with some quantitative predictions of the metallicities of binary stars as LGRB progenitors.

We emphasize that despite the vast and rich existing literature on star-forming galaxies, it was difficult to find comparison field galaxy samples whose completeness limits were suitable for comparison to LGRB hosts. Even at low and intermediate redshifts, the LGRB host population can thus be complementary to surveys studying the low-mass, faint galaxy population, in particular when extending the mass-metallicity (or FMR) relation to low stellar masses ($\sim 10^8$ $M_\odot$). LGRBs preferentially select metal-poor galaxies. It has been suggested that $M_\star$ and SFR are the main parameters driving the FMR, not metallicity (Hunt et al. 2012). This would mean that LGRBs select low-mass galaxies much more effectively than magnitude-limited surveys.

Although the sample of galaxies used in this study is small, we emphasize the importance of using complete samples to understand the properties of the LGRB host population. In the future we will move our analysis towards higher redshifts with the aim of obtaining a deeper insight into the condition affecting the rate of LGRBs to confirm if, as suggested by recent studies (Greiner et al. 2015; Perley et al. 2016b), LGRBs become direct SFR tracers as we move back through cosmic time.

Acknowledgements. We thank the referee for the helpful comments that improved the paper. S.D.V. thanks C. Belczynski, C.Georgy, J. Groh, O. Le Fèvre, L. Kewley and L. Tasca for fruitful discussions. J.J. and S.C. acknowledge financial contribution from the grant PRIN MIUR 2012 201278X4FL 002 The Intergalactic Medium as a probe of the growth of cosmic structures. S.D.V. and E.L.F. acknowledge the UnivEarthS Labex programme at Sorbonne Paris Cité (ANR-10-LABX-0023 and ANR-11-IDEX-0005-02). A.F.S. acknowledges support from grants AYA2013-48623-C2-2 from the Spanish Ministerio de Economia y Competitividad, and PrometeoII 2014/060 from the Generalitat Valenciana. This research uses data from the VIMOS VLT Deep Survey, obtained from the VVDS database operated by Cesam, Laboratoire d'Astrophysique de Marseille, France. This work is partly based on observations made with the Gran Telescopio Canarias (GTC), installed in the Spanish Observatorio del Roque de los Muchachos of the Instituto de Astrofísica de Canarias in the island of La Palma.

References

Atek, H., Malkan, M., McCarthy, P., et al. 2010, ApJ, 723, 104
Atek, H., Kneib, J.-P., Pacifici, C., et al. 2014, ApJ, 789, 96
Basa, S., Cuby, J. G., Savaglio, S., et al. 2012, A&A, 542, A103
Bianco, F. B., Modjaz, M., Oh, S. M., et al. 2015, Astron. Comput., submitted [arXiv:1505.06213]
Boissier, S., Salvaterra, R., Le Floc'h, E., et al. 2013, A&A, 557, A34
Brammer, G. B., van Dokkum, P. G., Franx, M., et al. 2012, ApJS, 200, 13
Brinchmann, J., Charlot, S., White, S. D. M., et al. 2004, MNRAS, 351, 1151
Cardelli, J. A., Clayton, G. C., & Mathis, J. S. 1989, ApJ, 345, 245
Carilli, C. L., & Walter, F. 2013, ARA&A, 51, 105
Chabrier, G. 2003, PASP, 115, 763
Christensen, L., Vreeswijk, P. M., Sollerman, J., et al. 2008, A&A, 490, 45
Covino, S., Melandri, A., Salvaterra, R., et al. 2013, MNRAS, 432, 1231
Cowie, L. L., & Barger, A. J. 2008, ApJ, 686, 72
Della Valle, M., Chincarini, G., Panagia, N., et al. 2006, Nature, 444, 1050
Filgas, R., Greiner, J., Schady, P., et al. 2011, A&A, 535, A57
Fong, W., & Berger, E. 2013, ApJ, 776, 18

Fruchter, A. S., Levan, A. J., Strolger, L., et al. 2006, Nature, 441, 463
Fynbo, J. P. U., Watson, D., Thöne, C. C., et al. 2006, Nature, 444, 1047
Fynbo, J. P. U., Jakobsson, P., Prochaska, J. X., et al. 2009, ApJS, 185, 526
Gehrels, N., Chincarini, G., Giommi, P., et al. 2004, ApJ, 611, 1005
Gil de Paz, A., Madore, B. F., & Pevunova, O. 2003, ApJS, 147, 29
Goldoni, P., Royer, F., François, P., et al. 2006, in SPIE Conf. Ser., 6269, 2
Graham, J. F., & Fruchter, A. S. 2013, ApJ, 774, 119
Greiner, J., Krühler, T., Klose, S., et al. 2011, A&A, 526, A30
Greiner, J., Fox, D. B., Schady, P., et al. 2015, ApJ, 809, 76
Hirschi, R., Meynet, G., & Maeder, A. 2005, A&A, 443, 581
Hjorth, J., & Bloom, J. S. 2012, in Gamma-Ray Bursts, Cambridge Astrophys. Ser. 51 (CUP), 169
Hjorth, J., Sollerman, J., Møller, P., et al. 2003, Nature, 423, 847
Hjorth, J., Malesani, D., Jakobsson, P., et al. 2012, ApJ, 756, 187
Huang, K. Y., Urata, Y., Tung, Y. H., et al. 2012, ApJ, 748, 44
Hunt, L., Magrini, L., Galli, D., et al. 2012, MNRAS, 427, 906
Hunt, L. K., Palazzi, E., Michałowski, M. J., et al. 2014, A&A, 565, A112
Hunt, L., Dayal, P., Magrini, L., & Ferrara, A. 2016, MNRAS, submitted
Ilbert, O., McCracken, H. J., Le Fèvre, O., et al. 2013, A&A, 556, A55
Jakobsson, P., Hjorth, J., Fynbo, J. P. U., et al. 2004, ApJ, 617, L21
Jakobsson, P., Levan, A., Fynbo, J. P. U., et al. 2006, A&A, 447, 897
Japelj, J., Covino, S., Gomboc, A., et al. 2015, A&A, 579, A74
Jin, Z.-P., Covino, S., Della Valle, M., et al. 2013, ApJ, 774, 114
Jin, Z.-P., Li, X., Cano, Z., et al. 2015, ApJ, 811, L22
Kausch, W., Noll, S., Smette, A., et al. 2015, A&A, 576, A78
Kelly, P. L., Filippenko, A. V., Modjaz, M., & Kocevski, D. 2014, ApJ, 789, 23
Kennicutt, Jr., R. C. 1998, ARA&A, 36, 189
Kewley, L. J., & Ellison, S. L. 2008, ApJ, 681, 1183
Kewley, L. J., Geller, M. J., & Jansen, R. A. 2004, AJ, 127, 2002
Kewley, L. J., Maier, C., Yabe, K., et al. 2013, ApJ, 774, L10
Kistler, M. D., Yüksel, H., Beacom, J. F., & Stanek, K. Z. 2008, ApJ, 673, L119
Kobulnicky, H. A., & Kewley, L. J. 2004, ApJ, 617, 240
Krühler, T., Malesani, D., Fynbo, J. P. U., et al. 2015, A&A, 581, A125
Le Fèvre, O., Saisse, M., Mancini, D., et al. 2003, in Instrument Design and Performance for Optical/Infrared Ground-based Telescopes, eds. M. Iye, & A. F. M. Moorwood, SPIE Conf. Ser., 4841, 1670
Le Fèvre, O., Vettolani, G., Garilli, B., et al. 2005, A&A, 439, 845
Le Fèvre, O., Cassata, P., Cucciati, O., et al. 2013, A&A, 559, A14
Le Floc'h, E., Duc, P.-A., Mirabel, I. F., et al. 2003, A&A, 400, 499
Le Floc'h, E., Charmandaris, V., Forrest, W. J., et al. 2006, ApJ, 642, 636
Levesque, E. M., Kewley, L. J., Berger, E., & Zahid, H. J. 2010a, AJ, 140, 1557
Levesque, E. M., Soderberg, A. M., Kewley, L. J., & Berger, E. 2010b, ApJ, 725, 1337
Levesque, E. M., Berger, E., Soderberg, A. M., & Chornock, R. 2011, ApJ, 739, 23
Li, L.-X., & Paczyński, B. 1998, ApJ, 507, L59
Ly, C., Lee, J. C., Dale, D. A., et al. 2011, ApJ, 726, 109
Maiolino, R., Nagao, T., Grazian, A., et al. 2008, A&A, 488, 463
Mannucci, F., Cresci, G., Maiolino, R., et al. 2009, MNRAS, 398, 1915
Mannucci, F., Cresci, G., Maiolino, R., Marconi, A., & Gnerucci, A. 2010, MNRAS, 408, 2115
Mannucci, F., Salvaterra, R., & Campisi, M. A. 2011, MNRAS, 414, 1263
Melandri, A., Sbarufatti, B., D'Avanzo, P., et al. 2012, MNRAS, 421, 1265
Michałowski, M. J., Kamble, A., Hjorth, J., et al. 2012, ApJ, 755, 85
Modigliani, A., Goldoni, P., Royer, F., et al. 2010, in SPIE Conf. Ser., 7737, 28
Modjaz, M., Kewley, L., Kirshner, R. P., et al. 2008, AJ, 135, 1136
Moustakas, J., Kennicutt, Jr., R. C., & Tremonti, C. A. 2006, ApJ, 642, 775
Nava, L., Salvaterra, R., Ghirlanda, G., et al. 2012, MNRAS, 421, 1256
Osterbrock, D. E., & Ferland, G. J. 2006, Astrophysics of gaseous nebulae and active galactic nuclei (Sausalito, CA: University Science Books)
Pei, Y. C. 1992, ApJ, 395, 130
Perley, D. A., Levan, A. J., Tanvir, N. R., et al. 2013, ApJ, 778, 128
Perley, D. A., Perley, R. A., Hjorth, J., et al. 2015, ApJ, 801, 102
Perley, D. A., Krühler, T., Schulze, S., et al. 2016a, ApJ, 817, 7
Perley, D. A., Tanvir, N. R., Hjorth, J., et al. 2016b, ApJ, 817, 8
Pescalli, A., Ghirlanda, G., Salvaterra, R., et al. 2016, A&A, 587, A40
Pettini, M., & Pagel, B. E. J. 2004, MNRAS, 348, L59
Piranomonte, S., Japelj, J., Vergani, S. D., et al. 2015, MNRAS, 452, 3293
Pita, S., Goldoni, P., Boisson, C., et al. 2014, A&A, 565, A12
Planck Collaboration XVI. 2014, A&A, 571, A16
Robertson, B. E., & Ellis, R. S. 2012, ApJ, 744, 95
Rodríguez-Muñoz, L., Gallego, J., Pacifici, C., et al. 2015, ApJ, 799, 36
Sakamoto, T., Sato, G., Barbier, L., et al. 2009, ApJ, 693, 922
Salvaterra, R., Ferrara, A., & Dayal, P. 2011, MNRAS, 414, 847
Salvaterra, R., Campana, S., Vergani, S. D., et al. 2012, ApJ, 749, 68
Salvaterra, R., Maio, U., Ciardi, B., & Campisi, M. A. 2013, MNRAS, 429, 2718
Savaglio, S., Glazebrook, K., Le Borgne, D., et al. 2005, ApJ, 635, 260
Savaglio, S., Glazebrook, K., & Le Borgne, D. 2009, ApJ, 691, 182
Schlafly, E. F., & Finkbeiner, D. P. 2011, ApJ, 737, 103
Schulze, S., Chapman, R., Hjorth, J., et al. 2015, ApJ, 808, 73
Shapley, A. E. 2011, ARA&A, 49, 525
Shapley, A. E., Reddy, N. A., Kriek, M., et al. 2015, ApJ, 801, 88
Smette, A., Sana, H., Noll, S., et al. 2015, A&A, 576, A77
Speagle, J. S., Steinhardt, C. L., Capak, P. L., & Silverman, J. D. 2014, ApJS, 214, 15
Steinhardt, C. L., Speagle, J. S., Capak, P., et al. 2014, ApJ, 791, L25
Svensson, K. M., Levan, A. J., Tanvir, N. R., Fruchter, A. S., & Strolger, L.-G. 2010, MNRAS, 405, 57
Tanvir, N. R., Rol, E., Levan, A. J., et al. 2010, ApJ, 725, 625
Tanvir, N. R., Levan, A. J., Fruchter, A. S., et al. 2012, ApJ, 754, 46
Tremonti, C. A., Heckman, T. M., Kauffmann, G., et al. 2004, ApJ, 613, 898
van Dokkum, P. G. 2001, PASP, 113, 1420
Vergani, S. D., Flores, H., Covino, S., et al. 2011, A&A, 535, A127
Vergani, S. D., Salvaterra, R., Japelj, J., et al. 2015, A&A, 581, A102
Vernet, J., Kerber, F., Mainieri, V., et al. 2010, Highlights of Astronomy, 15, 535
Vernet, J., Dekker, H., D'Odorico, S., et al. 2011, A&A, 536, A105
Whitaker, K. E., van Dokkum, P. G., Brammer, G., & Franx, M. 2012, ApJ, 754, L29
Whitaker, K. E., Franx, M., Leja, J., et al. 2014, ApJ, 795, 104
Wiersema, K., Curran, P. A., Krühler, T., et al. 2012, MNRAS, 426, 2
Woosley, S. E., & Heger, A. 2006, ApJ, 637, 914
Yang, B., Jin, Z.-P., Li, X., et al. 2015, Nature Commun., 6, 7323
Yoon, S.-C., Langer, N., & Norman, C. 2006, A&A, 460, 199
Zahid, H. J., Kewley, L. J., & Bresolin, F. 2011, ApJ, 730, 137
Zahid, H. J., Geller, M. J., Kewley, L. J., et al. 2013a, ApJ, 771, L19
Zahid, H. J., Yates, R. M., Kewley, L. J., & Kudritzki, R. P. 2013b, ApJ, 763, 92
Zahid, H. J., Dima, G. I., Kudritzki, R.-P., et al. 2014, ApJ, 791, 130

Appendix A

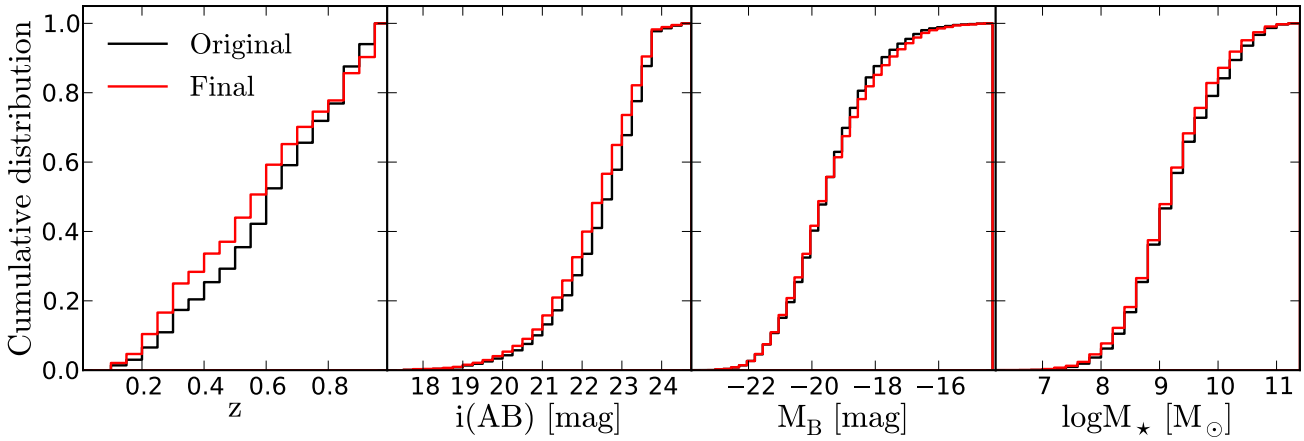

Fig. A.1. Cumulative plots of properties of the comparison galaxy sample from the VVDS survey illustrating that the original sample (6366 galaxies, black lines) and the final sample (3551 galaxies, red lines) that was used in the analysis do not differ in their properties and that no bias was introduced in the selection process.

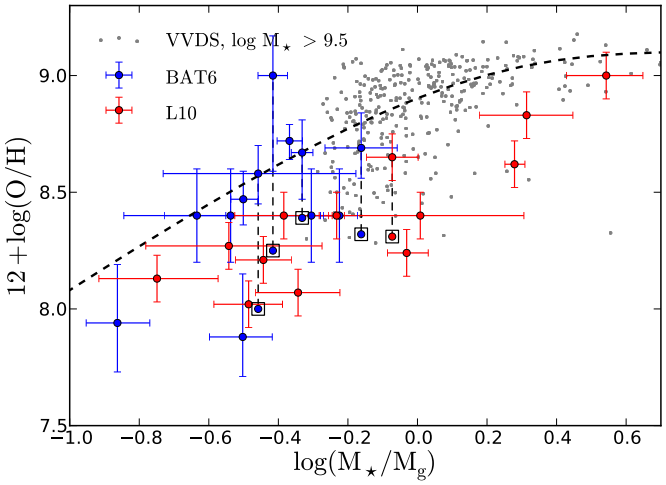

Fig. A.2. Relation between metallicity and stellar-to-gas mass ratio. Metallicity is given in the calibration of KK04. The dashed line is the relation found by Zahid et al. (2014) for star-forming galaxies. Gas (hydrogen) masses are computed using Eq. (34) in Zahid et al. (2014). Errors on the x-axis only take into account the errors on measured $M_\star$: the true errors are larger due to the error in metallicity calibration (~0.15 dex) and the scatter in the relation itself (~0.07 dex). Blue data show the BAT6 sample, red represent the Levesque et al. (2010a) sample, and grey dots the values computed from the VVDS sample (only log $M_\star > 9.5$, which allows the assumption that all correct KK04 values are of the upper branch). It is evident that the biased sample used by Levesque et al. (2010a) lies below the median relation of star-forming galaxies. While a few of our own LGRB hosts seem to be outliers, most of our hosts are consistent within errors with the relation.

Table A.1. Measured line fluxes (10^{-17} erg cm^{-2} s^{-1}), corrected for Galactic extinction and stellar Balmer absorption.

GRB	[O II][a]		[Ne III]	Hδ	Hγ	Hβ	[O III]		Hα	[N II]
	λ3726	λ3729					λ4959	λ5007		λ6584
050416A	4.3 ± 0.5	4.1 ± 0.5	<1.3	<1.0	1.1 ± 0.3	1.9 ± 0.4	1.8 ± 0.5	6.3 ± 0.5	11.8 ± 1.4	0.8 ± 0.3
050525A[i]	<1.7	<1.7	<2.0	<1.6	<2.0	[s]	1.2 ± 0.4	2.7 ± 0.4	2.2[h]	<2.5
060614	2.8 ± 0.5		<0.7	<1.2	<0.8	0.7 ± 0.2	[s]	2.8 ± 0.7	2.5 ± 0.5	<1.0
060912A	7.3 ± 0.4	10.8 ± 0.5	1.8 ± 0.5	0.7 ± 0.3	2.5 ± 0.3	5.3 ± 0.5	4.0 ± 0.5[t]	11.2 ± 1.2	17.4 ± 2.0	3.6 ± 2.5
061021	1.0 ± 0.2	1.0 ± 0.2	<0.6	<0.8	<2.1	0.5 ± 0.1	0.6 ± 0.1	1.7 ± 0.3	1.6 ± 0.3	<0.5
071112C[†]	1.9 ± 0.4		0.6 ± 0.2[s]	0.8 ± 0.4	1.2 ± 0.4	<2.0	2.5 ± 0.5	2.4 ± 0.5[t]		
080430	3.5 ± 0.8		2.3 ± 0.5	3.0 ± 0.7	[t]	4.7 ± 1.8	5.5 ± 1.2	[s]		
080916A	2.9 ± 0.4		[s]	<0.4	<0.5	1.8 ± 0.7[t]	[t]	3.6 ± 0.6		
081007	1.3 ± 0.2	1.6 ± 0.2	<1.4	<1.4	0.8 ± 0.2	1.4 ± 0.2	1.7 ± 0.2	5.9 ± 0.3	5.0 ± 0.3	[d]
090424	13.8 ± 2.3		[s]	[e]	1.7 ± 0.4	4.3 ± 0.6	1.3 ± 0.5[t]	3.5 ± 0.4	19.9 ± 3.3	[s]
091018[b,†]	1.7 ± 0.2	2.9 ± 0.4	[t]	<0.8	<0.8	1.3 ± 0.3[t]	1.7 ± 0.3	4.6 ± 1.0	5.6 ± 1.6[s]	<1.5
091127[†]	4.2 ± 0.7	5.4 ± 0.9	<1.4	0.7 ± 0.3	0.7 ± 0.2	2.3 ± 0.2	3.0 ± 0.2	7.8 ± 0.3	6.0 ± 0.3	0.5 ± 0.2
100621A	38.4 ± 5.4	49.0 ± 6.0	15.1 ± 3.2	11.4 ± 1.3	17.6 ± 1.3	38.0 ± 2.1	35.6 ± 1.1	130.4 ± 6.3	130.8 ± 11.5	9.7 ± 5.1[s]

Notes. Upper limits are estimated at 3σ level. No values are reported in cases where a line lies outside the covered spectral range or if it falls in the region of strong telluric absorption and is not detected. [(a)] If only one line is reported, the OII doublet is not resolved. [(b)] Hβ lies in a region a strong telluric absorption, but it is clearly detected. Telluric absorption was modelled with molecfit (Smette et al. 2015; Kausch et al. 2015) using the spectrum of the afterglow (has sufficiently high S/N) and applied to the spectrum. The corrected spectrum was used to measure Hβ. [(t)] Likely affected by (or, if no number, missing due to) significant telluric absorption. [(s)] Likely contaminated (or, if no number, completely dominated) by sky emission line residuals. [(d)] [N II]lies on the extremely noisy edge of the VIS spectral arm. [(e)] Hδ is observed in absorption. Balmer correction for this host is substantial. [(h)] The line is marginally detected but lies in a very noisy region. We measured its flux by fixing the centre and width of the Gaussian in the fit. The width was assumed to be the same as the one measured from the [O III]λ5007 line. [(i)] We note that Krühler et al. (2015) did not apply any additional correction to flux calibration for this host, given that the continuum is not detected. Our values of emission line fluxes are consistent with theirs before we applied the correction (Sect. 2.4). [(†)] Spectrum dominated by afterglow.